

Growth, crystal structure, and properties of epitaxial BiScO₃ thin films

Susan Trolier-McKinstry,^{1,a)} Michael D. Biegalski,² Junling Wang,³ Alexei A. Belik,⁴ Eiji Takayama-Muromachi,⁴ and Igor Levin⁵

¹Materials Science and Engineering Department, The Pennsylvania State University, University Park, Pennsylvania 16802, USA

²Center for Nanophase Materials Sciences, Oak Ridge National Laboratory, Oak Ridge, Tennessee 37830-6488, USA

³School of Materials Science and Engineering, Nanyang Technological University, Singapore 639798, Singapore

⁴International Center for Materials Nanoarchitectonics (MANA), National Institute for Materials Science (NIMS), 1-1 Namiki, Tsukuba, Ibaraki 305-0044, Japan

⁵Ceramics Division, National Institute of Standards and Technology, Gaithersburg, Maryland 20899, USA

(Received 19 March 2008; accepted 4 June 2008; published online 19 August 2008)

Epitaxial thin films of BiScO₃—a compound thermodynamically unstable under ambient conditions—were grown on BiFeO₃-buffered SrTiO₃ substrates. X-ray diffraction confirmed the reasonable crystalline quality of the films with a full width at half maximum of 0.58° in ω (004 reflection), 0.80° in ϕ (222 reflection), and 0.28° in θ . The epitaxial thin films of BiScO₃ on SrTiO₃ retain the principal structural features of bulk BiScO₃ (i.e., octahedral tilting and the pattern of Bi displacements) that give rise to a pseudo-orthorhombic unit cell $2\sqrt{2}a_c \times \sqrt{2}a_c \times 4a_c$ ($a_c \approx 4$ Å refers to the lattice parameter of an ideal cubic perovskite). Films grown on {100} substrates adopt the bulk monoclinic structure, whereas films on the (110) substrates appear to exhibit an orthorhombic symmetry. The dielectric permittivities were modest (≈ 30) with low loss tangents ($< 1\%$ at low fields); no maxima were observed over a temperature range of -200 to $+350$ °C. There is no evidence of significant hysteresis (either ferroelectric or antiferroelectric) at room temperature up to the breakdown strength of the films. © 2008 American Institute of Physics.

[DOI: [10.1063/1.2964087](https://doi.org/10.1063/1.2964087)]

INTRODUCTION

Ferroelectric lead zirconate titanate (PZT) ceramics are the basis for a large number of commercial piezoelectric devices.¹ Of particular interest are the superior properties found near the morphotropic phase boundary (MPB).² However, the relatively low Curie temperatures ($T_C \approx 380$ °C at the MPB) of the PZT system limit their utility in some applications. Moreover, the drive to move away from lead-containing piezoelectrics is spurring considerable research.

In the search for new high temperature or lead-free piezoelectrics, Bi-based perovskite compounds are of interest.³ Recently, $(1-x)\text{BiScO}_3-x\text{PbTiO}_3$ ceramics have been reported to exhibit piezoelectric properties ($d_{33} \sim 460$ pC/N) comparable to that of PZT and high ferroelectric transition temperature $T_C = 450$ °C near the MPB.^{4,5} Both single crystals⁶ and thin films⁷⁻⁹ also show good properties. Thin films of other BiScO₃ solid solutions have also been reported.^{10,11}

Despite its utility in ceramic solid solutions, there is little knowledge about the end member BiScO₃ itself. As a family, Bi-based ABO₃ perovskite-like oxides are attracting considerable attention because of their potentially exploitable functional properties. For example, BiFeO₃ (Ref. 12) and BiMnO₃ (Refs. 13 and 14) are multiferroics, whereas BiScO₃, as described above, is an interesting end member for both dielectric and piezoelectric solid solutions. Most of the

known BiBO₃ perovskites (including BiMnO₃ and BiScO₃) are unstable under ambient conditions, and their synthesis typically requires high pressures.^{15,16} This is likely due to a low structural stability for the perovskite phase that originates from the rather small tolerance factor.¹⁷ The crystal structures of BiFeO₃ (Ref. 18) and BiMnO₃ (Ref. 19) have been established. Recently, the structure of BiScO₃ synthesized under high pressure was determined using neutron powder diffraction and electron diffraction.^{20,21} According to these studies, BiScO₃ is isostructural with BiMnO₃ and exhibits a monoclinic $C2/c$ symmetry with lattice parameters $a = 9.889$ Å, $b = 5.822$ Å, $c = 10.046$ Å, and $\beta = 108.3^\circ$. Despite the existing knowledge of atomic positions, the origins of structural distortions (i.e., octahedral tilting, cation displacements, etc) that give rise to complex superstructures in both BiMnO₃ and BiScO₃ compounds have not been discussed. However, identifying these distortion mechanisms is essential both to an understanding of the displacive behavior in Bi-based perovskites as well as to the functional properties.²² In particular, it is not known at present whether BiScO₃ is ferroic. Although it has previously been speculated that it may be either ferroelectric or antiferroelectric, no experimental confirmation was reported.^{15,23,24} In the present work, these questions are addressed by stabilizing the perovskite phase in BiScO₃ thin films using epitaxy, thereby permitting structural and electrical characterization. The structure of thin films was compared to that of a bulk BiScO₃ sample synthesized under high pressure.²⁰

^{a)}Electronic mail: stmckinstry@psu.edu.

EXPERIMENTAL PROCEDURE

BiScO₃ films, BiFeO₃ buffer layers and SrRuO₃ bottom electrodes were all prepared on (100) and (110) SrTiO₃ single crystal substrates using pulsed laser deposition (PLD). A KrF excimer laser [Lambda Physik Compex 305i (the use of brand or trade names does not imply endorsement of the product by NIST)] with a 248 nm wavelength was used to ablate the target materials. The laser energy density used for BiScO₃ growth was $\approx 1.7\text{--}1.8$ J/cm². SrRuO₃ bottom electrodes and BiFeO₃ buffer layers were deposited using stoichiometric ceramic targets (Target Materials Inc.). Details of their epitaxial growth are given elsewhere.¹² BiScO₃ films were deposited using a mixed phase sintered ceramic target with 5 mol % excess Bi₂O₃ to compensate for the loss of bismuth during growth. The BiScO₃ target was sintered at 825 °C for 1 h.

(100) and (110) SrTiO₃ substrates (CrysTec GmbH) were first ultrasonically cleaned sequentially in trichloroethylene, acetone, and isopropanol and then mounted to the substrate heater with Ag paint. The chamber was pumped down to a base pressure of $10^{-5}\text{--}10^{-6}$ Torr and then backfilled with oxygen to the deposition pressure. The substrate was then heated to temperatures ranging from 500 to 800 °C. Following growth, the chamber pressure was increased to near an atmosphere of oxygen, and the samples were rapidly cooled to below 500 °C to minimize Bi volatilization.

The crystalline quality of the films was characterized by x-ray diffraction (XRD) using Cu K α radiation. θ - 2θ , ω , and ϕ scans were performed using a Scintag diffractometer and an X'Pert Philips four circle diffractometer. The crystal and domain structures of the BiScO₃ films were analyzed using transmission electron microscopy (TEM) and compared to those of the bulk BiScO₃ samples synthesized under high pressure. The TEM samples were prepared by conventional mechanical polishing and dimpling followed by ion thinning (at liquid nitrogen temperature) until perforation. For thin films, both cross-sectional and plane-view samples were used. Philips CM30 (200 kV) and JEOL 3010 UHR (300 kV) TEM instruments were used for diffraction and structural imaging, respectively.

Electrical characterization was performed either by patterning Pt top electrodes via a lift-off process and measuring through the film thickness or with interdigitated top electrodes for samples grown without a SrRuO₃ bottom electrode. This enabled measurement of the dielectric constant and loss (Hewlett Packard 4284A), as well as the polarization–electric field traces.

A rotating analyzer spectroscopic ellipsometer was used to determine the depth profile of the film stack, as well as the optical constants of the BiScO₃. Reference optical property data were used for the SrTiO₃ and SrRuO₃.^{25,26} Damped Sellmeier oscillators were used to describe BiScO₃ and BiFeO₃.

RESULTS AND DISCUSSION

Film growth

For initial growth runs in a background of 100 mTorr O₂, excess Bi₂O₃ was no longer detected at deposition tem-

peratures beyond 670 °C; thus, BiScO₃ was typically grown at 670 °C. As reported previously, for the growth conditions employed, phase pure perovskite BiScO₃ films could not be grown on SrTiO₃ or SrRuO₃/SrTiO₃ substrates.²⁷ Instead, diffraction peaks from Bi₂O₃ and Sc₂O₃ were detected with a trace of perovskite phase. Under the same growth conditions,²⁷ a thin BiFeO₃ buffer layer (5–10 nm) ameliorates this problem, as shown in Fig. 1. In this work, BiFeO₃ buffer layers of either 5 or 7.5 nm thickness were employed. The (001)_c orientation was obtained on (100) SrTiO₃, where the subscript *c* refers to an ideal cubic perovskite unit cell with $a_c \approx 4$ Å. The out-of-plane pseudocubic lattice constant was 4.137 ± 0.001 Å, which is larger than those reported for bulk ceramics. The full width at half maximum (FWHM) of the BiScO₃ 002_c and 222_c diffraction peaks in the θ - 2θ and ϕ scans were 0.28° and 0.8°, respectively. The fourfold periodicity of the ϕ scan of the BiScO₃ 222_c peaks demonstrates that cube on cube epitaxy was achieved.

Even with the BiFeO₃ buffer layer, it is observed that the growth rate (laser frequency) affects the film phase purity dramatically. Figure 2 shows the XRD patterns of samples that were grown at 670 °C (100 mTorr oxygen background) but with different laser frequencies. Clearly, the intermediate growth rate results in the best crystallinity and phase purity. At lower rates, a minor peak appears at $\approx 32^\circ$, which may come from a {110}-oriented perovskite phase or a second phase such as Sc₂O₃. The optimized growth condition was identified as $T_{\text{sub}}=670$ °C, 100 mTorr O₂ background pressure, and 10 Hz laser frequency.

BiScO₃ films were grown on {110} SrTiO₃ using the same deposition conditions. Out-of-plane XRD measurements show an excellent orientation for the BiScO₃, while the TEM measurements described below confirm epitaxy.

Structure determination

The reported BiScO₃ structure²⁰ reveals a coexistence of the two principal effects: (1) octahedral tilting and (2) anti-parallel Bi displacements similar to those of Pb in PbZrO₃.²⁸ The octahedra exhibit periodic antiphase tilting about two of the $\langle 001 \rangle_c$ directions, which results in the $\sqrt{2}a_c \times \sqrt{2}a_c \times 2a_c$ orthorhombic superlattice. Octahedral tilting about the third $\langle 001 \rangle_c$ direction parallel to the *c*-axis of this cell is irregular, being obscured by severe distortion of [ScO₆] octahedra (Fig. 3); therefore, the overall tilting topology in BiScO₃ cannot be easily described using Glazer notation.²⁹ Bi displacements, directed along the *b*-axis of the orthorhombic cell, double the periodicity along both *a*- and *c*-axes to yield $2\sqrt{2}a_c \times \sqrt{2}a_c \times 4a_c$. Hereafter, this orthorhombic cell will be denoted using a subscript *o*. The displacement patterns for Bi in the successive *c_o*-planes are illustrated in Fig. 4. A distinct sequence of Bi *c_o*-planes is supported by the oxygen displacements that take the form of periodic bending of octahedra (Fig. 3). The actual BiScO₃ structure is distorted from orthorhombic and exhibits a monoclinic symmetry with the lattice parameters $a_m \approx \sqrt{6}a_c$, $b_m \approx \sqrt{2}a_c$, $c_m \approx \sqrt{6}a_c$, and $\beta \approx 108^\circ$. The pseudo-orthorhombic and monoclinic lattices are related according to $\mathbf{a}_o = \mathbf{a}_m + \mathbf{c}_m$, $\mathbf{b}_o = \mathbf{b}_m$, and $\mathbf{c}_o = \mathbf{a}_m - \mathbf{c}_m$.

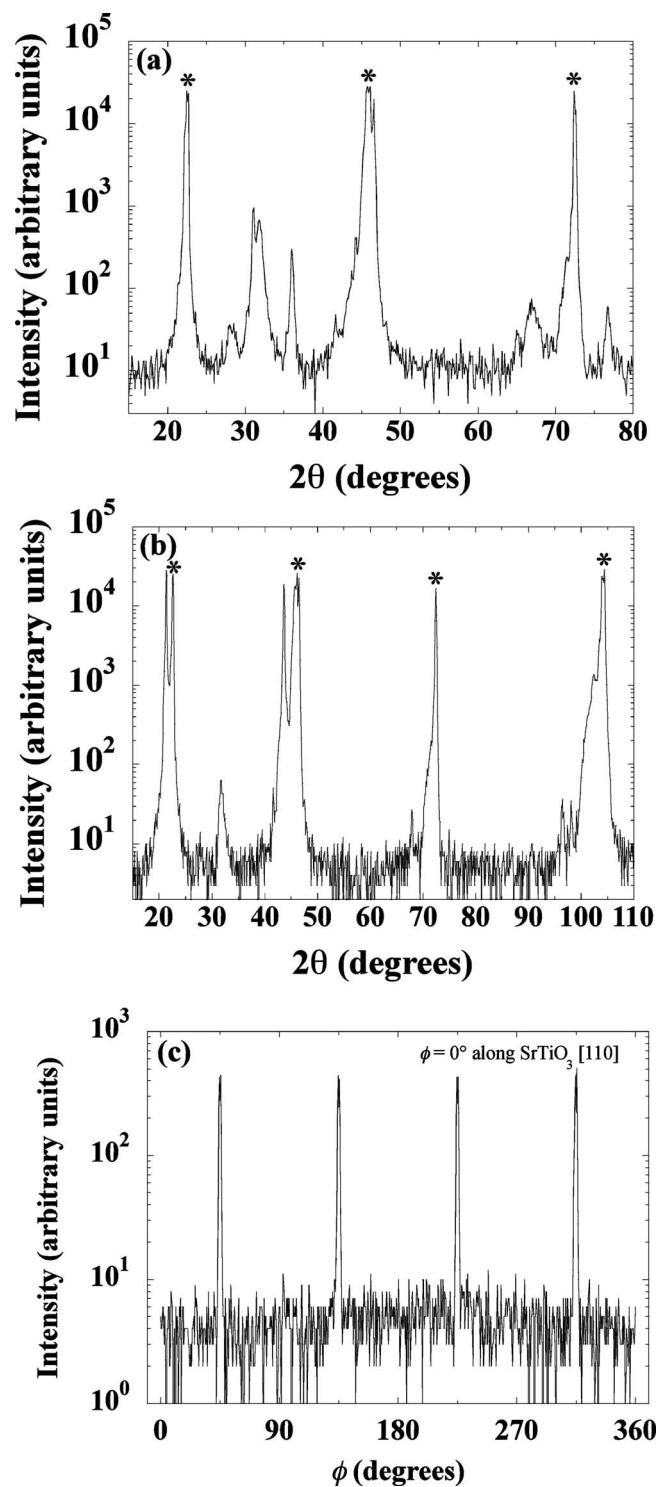


FIG. 1. XRD for BiScO₃ films grown on (a) SrRuO₃/SrTiO₃ {100} and (b) BiFeO₃/SrRuO₃/SrTiO₃ {100} substrates. The depositions were done at a substrate temperature of 670 °C, an oxygen pressure of 100 mTorr, and a laser frequency of 10 Hz. (c) ϕ scan of the BiScO₃ 222_c reflection for the same film shown in (b). Peaks with an asterisk are from the SrTiO₃ substrate.

The room-temperature lattice parameters of BiScO₃ in the orthorhombic setting are $a_o=11.676$ Å, $b_o=5.822$ Å, $c_o=16.159$ Å, and $\beta=90.95^\circ$.

As a reference for the thin films, electron diffraction patterns from a bulk BiScO₃ pellet were collected. BiScO₃ pellets were prepared by cold pressing of a powder sample at

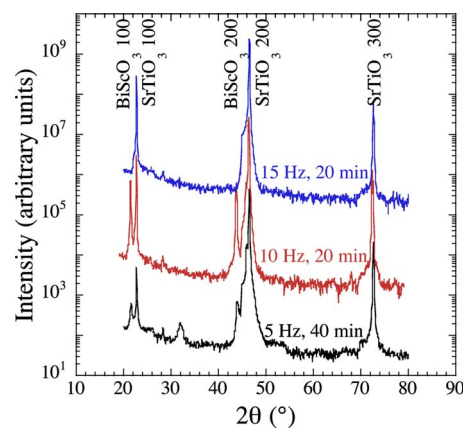


FIG. 2. (Color online) XRD of BiScO₃ films grown on BiFeO₃/SrRuO₃/SrTiO₃ {100} substrates at a substrate temperature of 670 °C and an oxygen pressure of 100 mTorr. The laser frequency (growth rate) dramatically changes the film phase and crystallinity. The reflections are indexed according to the pseudocubic unit cell.

about 2.5 GPa. The synthesis of these samples is described elsewhere.²⁰ Selected area electron diffraction patterns (Figs. 5 and 6) for the bulk sample support the $C2/c$ monoclinic structure deduced previously from x-ray and neutron powder diffraction data. Lack of the regular *in-phase* octahedral tilting is evident from the absence of the $\frac{1}{2}hk0_c$ ($h=2n+1$ and $k=2n+1$) reflections. Individual grains in this sample contained multiple rotational (twin-type) variants of the monoclinic cell (Fig. 7). The diffraction patterns revealed nearly continuous relrods (streaks) of diffuse intensity parallel to the c_o -axis ($4a_c$) of the pseudo-orthorhombic cell (i.e., $[10\bar{1}]_m$ monoclinic axis) passing through the hhl_m ($l=2n$) reflections (Figs. 5 and 6). Dark-field imaging (Fig. 7) confirmed that these relrods are associated with a high incidence of planar defects, which can be attributed to the antiphase shifts for the directions of Bi displacements in successive c_o -planes. Nonzero intensities at $\mathbf{k}=\frac{1}{4}[110]_c^*$ (asterisk indicates reciprocal space) presumably arise from the intersection of these relrods with the Ewald sphere (Fig. 6), as confirmed by tilting the crystals around both a_o or b_o axes. Some additional disorder in the directions of Bi displacements within the c_o -planes is reflected in the diffuse streaking along the $[101]_m/[100]_o$ direction.

The reciprocal lattices of both $\{001\}_c$ - and $\{110\}_c$ -oriented films, reconstructed from the series of electron diffraction patterns, were consistent with the pseudo-

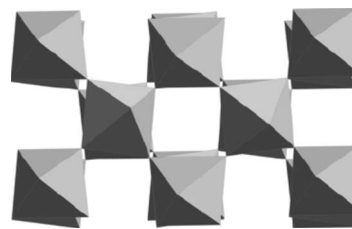


FIG. 3. A projection of the octahedral framework in the BiScO₃ structure along the $[101]$ direction of the $C2/c$ cell (parallel to the c -axis of the orthorhombic cell $2\sqrt{2}a_c \times \sqrt{2}a_c \times 4a_c$). Octahedral tilting about the viewing direction is very irregular due to a pronounced distortion of the $[\text{ScO}_6]$ octahedra.

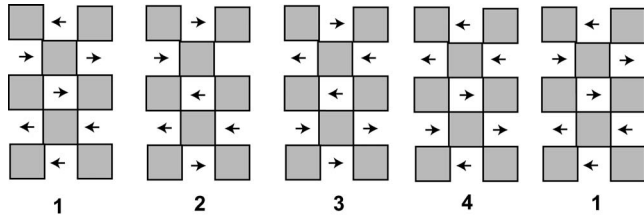


FIG. 4. Patterns of Bi displacements (indicated using arrows) in the successive c_o -layers of the bulk BiScO_3 structure.

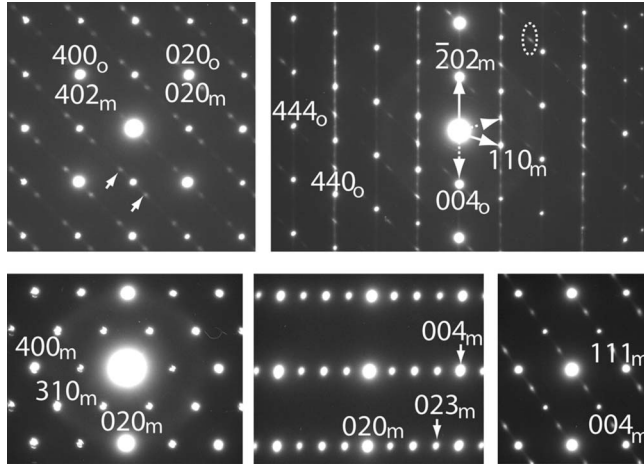


FIG. 5. Representative selected area electron diffraction patterns recorded from the bulk BiScO_3 sample. The patterns are indexed according to the monoclinic and pseudo-orthorhombic cells. The diffuse spots indicated using arrows in the $[\bar{1}02]_m$ pattern were attributed to the intersection of diffuse relrods parallel to $[001]_o$, which are seen clearly in the $[\bar{1}1\bar{1}]_m$ orientation, with the $[102]_m$ section of reciprocal lattice. Similarly, the weak reflections encircled using a dotted line in the $[\bar{1}1\bar{1}]_m$ pattern can be attributed to the intersection of such diffuse relrods from another twin variant (having orthogonal c_o -axis) with the $[\bar{1}1\bar{1}]_m$ reciprocal lattice section. Two monoclinic variants with parallel b_m -axes contribute to the $[\bar{1}1\bar{1}]_m$ pattern, as indicated using solid and dotted arrows, respectively.

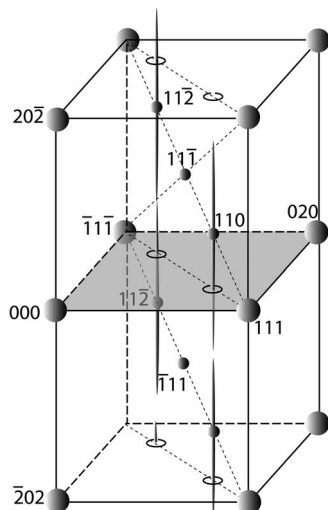


FIG. 6. Schematic representation of the reciprocal lattice for a single domain of BiScO_3 in the bulk sample. The diffuse streaks of intensity are clearly observed in the $[\bar{1}1\bar{1}]_m$ diffraction pattern in Fig. 5.

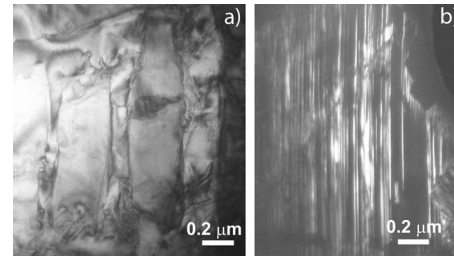


FIG. 7. Diffraction contrast images of individual grains in the bulk BiScO_3 sample. (a) Bright-field image reveals twin domains representing variants of the pseudo-orthorhombic cell with orthogonal c_o -axes. (b) Dark-field image recorded with the 110_m reflections highlights the high density of planar interfaces on the $(001)_o \parallel (\bar{2}02)_m$ planes that represent antiphase and monoclinic twin-domain boundaries.

orthorhombic cell of the bulk BiScO_3 , $2\sqrt{2}a_c \times \sqrt{2}a_c \times 4a_c$ (Fig. 8). However, the domain structures and details of structural distortions varied markedly with the orientation of SrTiO_3 , as described below.

BiScO_3 films grown on (100) SrTiO_3 yield electron diffraction patterns similar to those from the bulk samples (Fig. 9). The films consist of four twin-related variants of the orthorhombic structure (Fig. 10). For each domain, the a_o - and b_o -axes are parallel to the out-of-plane $\langle 101 \rangle_c$ directions, while the c_o -axis ($4a_c$) is parallel to the *in-plane* $\langle 100 \rangle_c$ direction (Fig. 8). No domains with the out-of-plane c_o -axis were observed. Clear and reproducible intensity variations among the 111_o and $11\bar{1}_o$ reflections are consistent with the monoclinic symmetry adopted by the bulk structure. Similar to the bulk samples, films on $\{100\}$ SrTiO_3 exhibit a high incidence of planar interfaces (monoclinic twin domain boundaries and antiphase defects) that generate streaks of diffuse intensity along the c_o -axis.

In contrast to the films on $\{100\}$ substrates, the BiScO_3 films on $\{110\}$ SrTiO_3 feature a single orthorhombic variant having a_o - and c_o -axes parallel to the *out-of-plane* $\langle 110 \rangle_c$ and *in-plane* $\langle 100 \rangle_c$ directions, respectively (Figs. 8 and 11). For these films (Fig. 11), no obvious signatures of monoclinic distortion were observed (note the similar intensity of the 111_o and $11\bar{1}_o$ reflections). Similar to the bulk samples and films, the relrods of diffuse intensity pass through the superlattice reflections parallel to the c_o -axis. The principal differ-

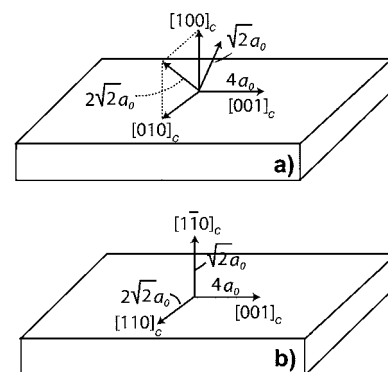


FIG. 8. Schematic representation of the orientation relations between the BiScO_3 film and the (a) $\{100\}$ and (b) $\{110\}$ SrTiO_3 substrates. In (a), only one (out of four) rotational variants of BiScO_3 is indicated for clarity.

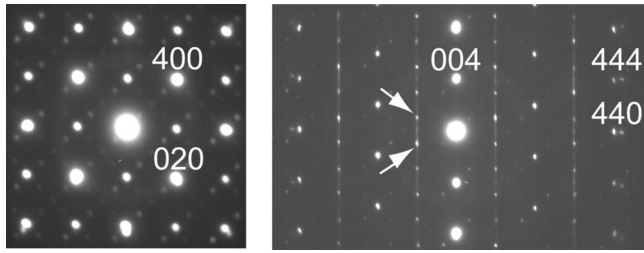


FIG. 9. Selected area electron diffraction patterns recorded from the BiScO₃ film on {100} SrTiO₃. The reflections are indexed according to the orthorhombic $2\sqrt{2}a_c \times \sqrt{2}a_c \times 4a_c$ unit cell. Note the intensity variance among the 111 and $11\bar{1}$ reflections (indicated using arrows), as well as the diffuse streaking through the hhl ($l=2n$) reflections.

ence between the reciprocal lattices of the $\{110\}_c$ and $\{100\}_c$ films is associated with the presence of strong sharp hhl_o ($l=2n$) and weak diffuse hhl_o ($l=2n+1$) reflections in the former (the opposite is observed for the $\{100\}_c$ films), which suggests a dissimilar symmetry of the two types of films. These differences in the symmetry can be attributed to distinct stacking sequences of the Bi planes (Fig. 4) along the c_o -axis. Evidently, both types of films, as well as the bulk structure, exhibit a pronounced tendency toward the formation of the c_o -plane stacking defects (Fig. 12) as reflected in the presence of the c_o -axis diffuse relrods in all BiScO₃ samples. Assuming Bi displacements along the b -axis, as in the bulk structure, Bi displacements in the BiScO₃ thin films are directed out of the film plane, regardless of substrate orientation.

Electrical and optical characterization

Spectroscopic ellipsometry was used to analyze the depth profile of typical samples. Reference dielectric func-

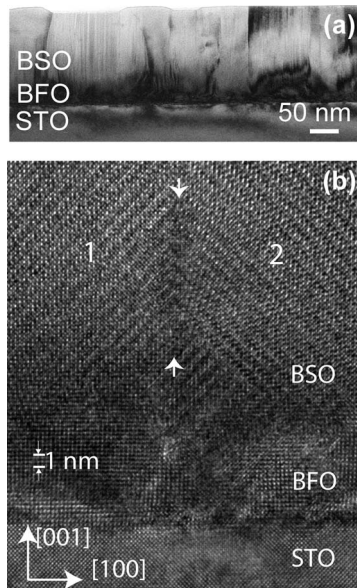


FIG. 10. (a) Cross-sectional bright-field image of the $\{001\}_c$ BiScO₃ film tilted about the surface normal away from the $\langle 100 \rangle_c$ zone axis orientation. Note the contrast striations that correspond to the planar defects perpendicular to the substrate. (b) Structural image showing epitaxial relation among the BiScO₃ film and the substrate. Two twin-related domains of the BiScO₃ structure are indicated as "1" and "2." The thin BiFeO₃ layer was not uniform across the substrate. In this figure BSO=BiScO₃, BFO=BiFeO₃, and STO=SrTiO₃.

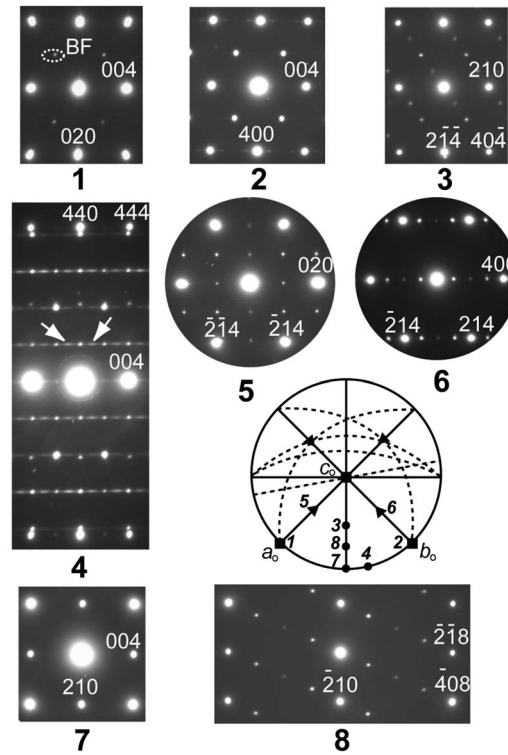


FIG. 11. Selected area electron diffraction patterns recorded from the BiScO₃ film on $\{110\}$ SrTiO₃. The reflections are indexed according to the orthorhombic $2\sqrt{2}a_c \times \sqrt{2}a_c \times 4a_c$ unit cell. The zone axis orientations are indicated using a stereographic projection. Reflections in the diffraction pattern (1) labeled as BF arise from the BiFeO₃ buffer layer. Note similar intensities of the 111_o and $11\bar{1}_o$ reflections and the diffuse nature of the hhl_o ($l=2n+1$) reflections in the diffraction pattern (4).

tion data were first obtained for BiFeO₃ from thin film BiFeO₃ samples grown on SrTiO₃. These data were then used to model a BiScO₃/BiFeO₃/SrTiO₃ stack. It was found that over the wavelength range from 350 to 650 nm, the optical properties of BiScO₃ could be well described by

$$\varepsilon = 1 + \frac{A\lambda^2}{\lambda^2 - \lambda_o^2}, \quad (1)$$

where λ is the wavelength in nanometers, ε is the dielectric function, $A=3.81 \pm 0.15$, and $\lambda_o=237.1 \pm 8.8$ nm. No improvement in the fit to the data was obtained by adding

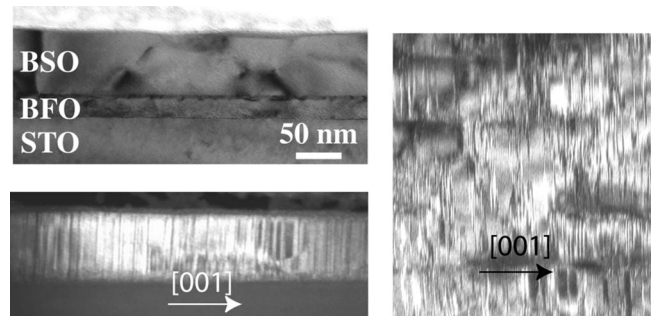


FIG. 12. Upper left: Cross-sectional bright-field image of the $\{110\}_c$ BiScO₃ film. Lower left: Cross-sectional dark-field image recorded with the hhl_o ($l=2n+1$) reflections. Right: Plane-view dark-field image recorded with the hhl_o ($l=2n+1$) reflections.

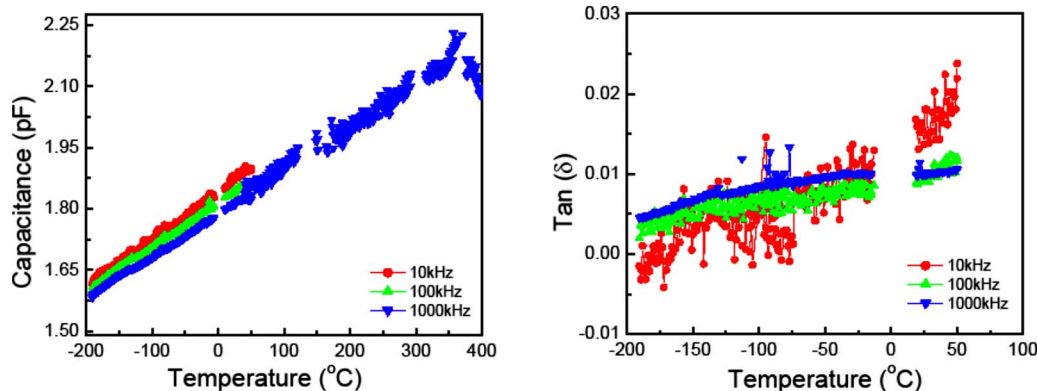


FIG. 13. (Color online) Temperature dependence of capacitance and dielectric loss of a Pt/BiScO₃/BiFeO₃/SrRuO₃/ {100} SrTiO₃ sample.

damping to the oscillator. It was also found that the films were extremely smooth, with well-defined interfaces; the modeled thicknesses for the BiFeO₃ and BiScO₃ were within experimental error of measurements made by other techniques.

Figure 13 shows the capacitance and loss tangent between -200 and 400 °C for a Pt/BiScO₃/BiFeO₃/SrRuO₃/ {100} SrTiO₃ sample. There is little dispersion in the dielectric constant, and the dielectric loss was low over the entire measurement range, suggesting that BiScO₃ is a good electrical insulator to at least 400 °C. The capacitance data, coupled with an estimated BiFeO₃ permittivity along $\langle 001 \rangle_c$ of 70,¹² was used to estimate the BiScO₃ permittivity. It was found for films on {100} substrates that the BiScO₃ films had permittivity measured through the film thickness between 22 and 36 (for 80 nm thick films). The calculated values lie between 21 and 34 if the BiFeO₃ is assumed to be conducting. This value is approximately half that of the reported value for ceramic samples. A 245 nm thick film deposited on (110) SrTiO₃ had a room-temperature dielectric constant of approximately 57 (calculated using a zero field permittivity for the BiFeO₃ film along $[110]_c$ of 90). The slight increase in the dielectric constant with increasing temperature could arise either from a possible phase transition at temperatures beyond 400 °C or potentially from the BiFeO₃. However, the smooth increase in permittivity with temperature suggests that there are no ferroic phase transitions in the BiScO₃ between -200 and $+350$ °C.

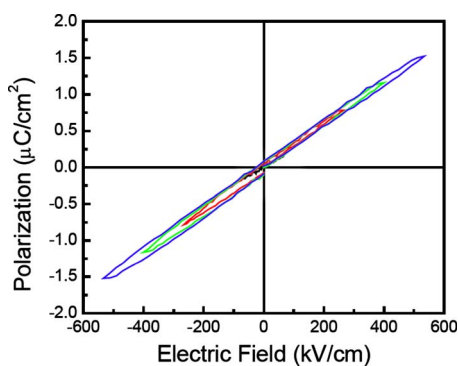


FIG. 14. (Color online) Dependence of polarization on electric field for a 160 nm thick BiScO₃ film on a 5 nm BiFeO₃/SrRuO₃/ {100} SrTiO₃ stack.

Higher electric fields were applied both on samples with top and bottom electrodes and on samples with interdigitated top electrodes only in an attempt to investigate whether the samples show any characteristic switchable polarization. As can be seen in Fig. 14, there was no detectable ferroelectric or antiferroelectric behavior that developed out of plane at electric fields up to 550 kV/cm for samples on {100} SrTiO₃. Instead the sample acted as a linear capacitor with a small dielectric loss at room temperature to the available range of field levels. The slope of the curve was consistent with the low field permittivity values. At 60 °C, there was no significant difference in the shape of the curves, except for an increase in the loss. Similarly, measurements made in plane on films on {100} SrTiO₃ showed no clear ferroelectric or antiferroelectric characteristics at room temperature (although in this case, only 50 kV/cm could be applied and the electric field will be poorly confined in the BiScO₃ layer).

To conclude, epitaxial BiScO₃ films were grown on BiFeO₃-buffered SrRuO₃/SrTiO₃. The results suggest that the epitaxial thin films of BiScO₃ on SrTiO₃ retain the principal structural features of the bulk ceramics synthesized at high pressures (i.e., octahedral tilting and patterns of Bi displacements) that give rise to a pseudo-orthorhombic unit cell $2\sqrt{2}a_c \times \sqrt{2}a_c \times 4a_c$. However, substrate orientation modifies details of the structural distortion along with the types and configurations of the twin domains: films on {100} SrTiO₃ adopt the bulk monoclinic structure, whereas the films on {110} SrTiO₃ appear to exhibit an orthorhombic symmetry. Similar to the bulk structure, all BiScO₃ films exhibit a pronounced disorder of Bi displacements. No phase transitions were apparent in the dielectric data between -200 and $+350$ °C. The effective permittivity for a stack of 10 nm of BiScO₃ on 5 nm of BiFeO₃ was 35 ± 3 .

ACKNOWLEDGMENTS

Support for this research was provided by the National Science Foundation (DMR-0602770). The film growth was conducted by STM while on sabbatical leave in the laboratories of R. Ramesh. Helpful discussions with Ichiro Takeuchi (U. Maryland) are also gratefully acknowledged. Vladimir Sherman (EPFL, Lausanne, Switzerland) and Beth Jones (Penn State) were extremely helpful in low temperature dielectric measurements and target preparation, respec-

tively. M.D.B. gratefully acknowledges support from the Division of Scientific User Facilities, Basic Energy Sciences, U.S. Department of Energy.

- ¹*Piezoelectric Materials in Devices*, edited by N. Setter (Nava Setter, Lausanne, Switzerland, 2002).
- ²B. Jaffe, W. R. Cook, and H. Jaffe, *Piezoelectric Ceramics* (Academic, New York, 1971).
- ³G. A. Smolenskii, V. A. Isupov, A. I. Agaranovskaya, and N. N. Krainik, *Sov. Phys. Solid State* **2**, 2651 (1961).
- ⁴R. E. Eitel, C. A. Randall, T. R. Shrout, P. W. Rehrig, W. Hackenberger, and S.-E. Park, *Jpn. J. Appl. Phys., Part 1* **40**, 5999 (2001).
- ⁵R. E. Eitel, C. A. Randall, T. R. Shrout, and S.-E. Park, *Jpn. J. Appl. Phys., Part 1* **41**, 2099 (2002).
- ⁶S. Zhang, L. Lebrun, S. Rhee, R. E. Eitel, C. A. Randall, and T. R. Shrout, *J. Cryst. Growth* **236**, 210 (2002).
- ⁷T. Yoshimura and S. Trolier-McKinstry, *Appl. Phys. Lett.* **81**, 2065 (2002).
- ⁸J. C. Nino and S. Trolier-McKinstry, *J. Mater. Res.* **19**, 568 (2004).
- ⁹H. Wen, X. H. Wang, X. Y. Deng, T. Y. Sun, and L. T. Li, *J. Appl. Phys.* **101**, 016103 (2007).
- ¹⁰S. Yasui, H. Uchida, H. Nakaki, H. Funakubo, and S. Koda, *Jpn. J. Appl. Phys., Part 1* **45**, 7321 (2006).
- ¹¹D. S. Tinberg and S. Trolier-McKinstry, *J. Appl. Phys.* **101**, 024112 (2007).
- ¹²J. Wang, J. B. Neaton, H. Zheng, V. Nagarajan, S. B. Ogale, B. Liu, D. Viehland, V. Vaithyanathan, D. G. Schlom, U. V. Waghmare, N. A. Spaldin, K. M. Rabe, M. Wuttig, and R. Ramesh, *Science* **299**, 1719 (2003).
- ¹³N. A. Hill and K. M. Rabe, *Phys. Rev. B* **59**, 8759 (1999).
- ¹⁴A. M. dos Santos, S. Parashar, A. R. Raju, Y. S. Zhao, A. K. Cheetham, and C. N. R. Rao, *Solid State Commun.* **122**, 49 (2002).
- ¹⁵Y. Y. Tomashpol'skii, E. V. Zubova, K. P. Burdina, and Y. N. Venetsev, *Sov. Phys. Crystallogr.* **13**, 859 (1969).
- ¹⁶Y. Y. Tomashpol'skii and Y. N. Venetsev, *Inorg. Mater.* **5**, 1087 (1969).
- ¹⁷R. D. Shannon, *Acta Crystallogr.* **32**, 751 (1976).
- ¹⁸F. Kubel and H. Schmid, *Acta Crystallogr., Sect. A: Found. Crystallogr.* **46**, 698 (1990).
- ¹⁹T. Atou, H. Chiba, K. Ohoyama, Y. Yamaguchi, and Y. Syono, *J. Solid State Chem.* **145**, 639 (1999).
- ²⁰A. A. Belik, S. Iikubo, K. Kodama, N. Igawa, S. Shamoto, M. Maie, T. Nagai, Y. Matsui, S. Y. Stefanovich, B. I. Lazoryak, and E. Takayama-Muromachi, *J. Am. Chem. Soc.* **128**, 706 (2006).
- ²¹T. Yokosawa, A. A. Belik, T. Asaka, K. Kimoto, E. Takayama-Muromachi, and Y. Matsui, *Phys. Rev. B* **77**, 024111 (2008).
- ²²R. Eitel and C. A. Randall, *Phys. Rev. B* **75**, 094106 (2007).
- ²³J. Iniguez, D. Vanderbilt, and L. Bellaiche, *Phys. Rev. B* **67**, 224107 (2003).
- ²⁴S. V. Halilov, M. Fornari, and D. J. Singh, *Phys. Rev. B* **69**, 174107 (2004).
- ²⁵B. J. Gibbons and S. Trolier-McKinstry, *IEEE Trans. Appl. Supercond.* **7**, 2177 (1997).
- ²⁶S. Trolier-McKinstry (unpublished).
- ²⁷M. Murakami, M. A. Aronova, M. Wuttig, I. Takeuchi, S. Trolier-McKinstry, K. McDonald, E. Knoesel, S. E. Lofland, T. Chikyow, T. Aoyama, and K. Nakajima, *Philos. Mag. Lett.* **87**, 241 (2007).
- ²⁸F. Jona, G. Shirane, F. Mazzi, and R. Pepinsky, *Phys. Rev.* **105**, 849 (1957).
- ²⁹A. M. Glazer, *Acta Crystallogr., Sect. B: Struct. Crystallogr. Cryst. Chem.* **28**, 3384 (1972).